SCIENTIFIC REPORTS

OPEN

Fine Tuning the Energy Barrier of Molecular Nanomagnets *via* Lattice Solvent Molecules

Received: 3 October 2017
Accepted: 2 November 2017
Published online: 14 November 2017

Cai-Ming Liu, De-Qing Zhang & Dao-Ben Zhu

Solvents play important roles in our lives, they are also of interest in molecular materials, especially for molecular magnets. The solvatomagnetic effect is generally used for trigger and/or regulation of magnetic properties in molecule-based systems, however, molecular nanomagnets showing solvatomagnetic effects are very difficult to obtain. Here we report four 3d-4f heterometallic cluster complexes containing ROH lattice solvent molecules, $[Cu_3Tb_2(H_3L)_2(OAc)_2(hfac)_4]\cdot 2ROH$ {H_6L = 1,3-Bis[tris(hydroxymethyl)methylamino]propane, $hfac^-$ = hexafluoroacetylacetonate; R = CH_3, 1; R = C_2H_5, 2; R = C_3H_7, 3; R = H, 4}. Single-molecule magnet (SMM) properties of these four complexes were observed to be dependent on the ROH lattice solvent molecule. There is an interesting magneto-structural correlation: the larger the R group, the higher the energy barrier. For the first time, the solvatomagnetic effect is used for the continuous fine adjustment of the energy barrier of 0D molecular nanomagnets. Additionally, $[Cu_3Dy_2(H_3L)_2(OAc)_2(hfac)_4]\cdot 2MeOH$ (5), an analogue of $[Cu_3Tb_2(H_3L)_2(OAc)_2(hfac)_4]\cdot 2MeOH$ (1), is also reported for comparison.

Solvents, especially water, are critical to the origins of life, and they have penetrated into all aspects of human life. Besides as reaction mediums and extracting agents, chemical solvents are also of interest in molecular materials. For example, in the field of molecular magnets they can be utilized as the terminal ligand to complete the coordination configuration[1–4]; and they can also serve as guest or lattice molecules to adjust magnetic properties[5–9]. The solvatomagnetic effect is very interesting because solvent molecules can be used for trigger and/or regulation of magnetic properties while the molecular magnetic structure is always maintained. Therefore, molecular magnets showing solvatomagnetic effects can be used as molecule devices, molecular switches and/or molecular sensors. Naturally, solvatomagnetic effects are often found in porous metal-organic frameworks (MOFs) in which solvent molecules are guest molecules[5–9], while low-dimensional systems with solvatomagnetic effects are more difficult to obtain due to the lack of pores. Recently, we found a chain-like azido-bridged manganese(III) coordination polymer showing both solvatomagnetic effect and spin-glass behaviour[10]. In studies of single molecule magnets (SMMs)[11], we also hope to explore SMM systems with solvatomagnetic effects. However, it is a great challenging task because most SMMs reported are concentrated on zero-dimensional (0 D) cluster or mononuclear systems.

It is well known that SMMs are of great potential for technological applications in high-density information storage, quantum computing and spintronics[12–17]; and the energy barrier leading to magnetic bistability and slow magnetic relaxation is a pivotal parameter. Therefore, except enhancing the relaxation energy barrier and increasing the blocking temperature[18–21], tuning the relaxation energy barrier is another important target in the molecular nanomagnet field[22–26]. Surprisingly, systematic studies of SMMs with the same magnetic structure are still rare, however, some factors such as the electron-withdrawing effect[27], the electrostatic potential of the key coordination atom[28] have been observed to be able to modulate SMMs' energy barriers recently. Regarding structures and magnetic properties may be affected by a small change of circumstance, solvent molecules may also be used to adjust SMMs' properties. To the best of our knowledge, a direct correlation between energy barriers and different lattice solvent molecules of 0D molecular nanomagnets has never been documented, though a 3D Dy(III) MOF-type SMM was found to show an obvious solvatomagnetic effect in 2015[29], and guest-dependent single-ion magnet behaviours were observed in a 2D cobalt(II) coordination polymer in 2016[30]. Herein we describe the lattice-solvent effect of ROH molecules (R = CH_3, **1**; R = C_2H_5, **2**; R = C_3H_7, **3**; R = H, **4**) on the energy barrier

Beijing National Laboratory for Molecular Sciences, Center for Molecular Science, Key Laboratory of Organic Solids, Institute of Chemistry, CAS Research/Education Center for Excellence in Molecular Science, Chinese Academy of Sciences, No. 2 1st North Street, Zhongguancun, Beijing, 100190, China. Correspondence and requests for materials should be addressed to C.-M.L. (email: cmliu@iccas.ac.cn)

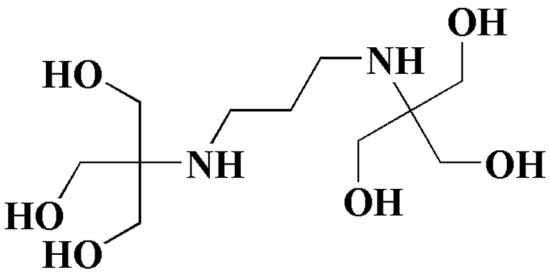

Figure 1. Molecular structure of H_6L.

of 0D SMMs with the same magnetic structure $[Cu_3Tb_2(H_3L)_2(OAc)_2(hfac)_4]$ {H_6L = 1,3-Bis[tris(hydroxymethyl)methylamino]propane, Fig. 1; $hfac^-$ = hexafluoroacetylacetonate}. Fine adjustment of the energy barrier (from 25.7 K to 33.1 K, H_{dc} = 0 Oe) in this $[Cu_3Tb_2(H_3L)_2(OAc)_2(hfac)_4]$ SMM system was achieved by changing the ROH lattice solvent molecule. A similar $[Cu_3Dy_2(H_3L)_2(OAc)_2(hfac)_4]$ SMM system was also studied, but only the crystal structure of $[Cu_3Dy_2(H_3L)_2(OAc)_2(hfac)_4]\cdot 2MeOH$ (**5**) was successfully solved; complex **5** also exhibits slow magnetic relaxation under zero dc field, with the energy barrier of 30.0 K, a relatively high value for reported relaxation barriers of the Cu-Dy heterometallic SMMs.

Results and Discussion

Preparation. Bis-tris propane (H_6L), an universal ligand due to flexible polydentate coordination sites, has been used to bind not only 3d transition metal ions[31,32] but also 4 f lanthanide metal ions[33]. Furthermore, it can also be utilized to construct 3d-4f heterometallic complexes[34]. Recently, Murrie *et al.* reported a series of 3d-4f complexes formulated as $\{Ln_2Cu_3(H_3L)_2X_n\}$ (X = OAc^-, Ln = Gd, Tb or X = NO_3^-, Ln = Gd, Tb, Dy, Ho, Er)[35]; they found that changing the auxiliary ligand OAc^- through NO_3^- may lead to a remarkable improvement of the energy barrier of $\{Tb_2Cu_3(H_3L)_2X_n\}$ (X = OAc^- and NO_3^-) complexes, which suggests that the anion co-ligand has a great impact on the energy barrier of $\{Tb_2Cu_3(H_3L)_2X_n\}$ SMMs. In the recent process of pursuing new SMMs, we observed that using $Ln(OAc)(hfac)_2(H_2O)_2$ as the lanthanide (III) salt source may lead mixed co-ligands OAc^- and $hfac^-$ into 3d-4f heterometallic clusters effectively[36]. Therefore, we adopted this synthesis strategy to obtain the $[Cu_3Tb_2(H_3L)_2(OAc)_2(hfac)_4]$ SMM with different ROH lattice solvent molecules (methanol, ethanol and isopropyl alcohol), in which not only the OAc^- anion but also the $hfac^-$ anion are co-ligands. Notably, our synthetic procedures were completed at room temperature rather than at 60 °C used by Murrie group[35]. Products using methanol, ethanol and isopropyl alcohol as reaction solvents were $[Cu_3Tb_2(H_3L)_2(OAc)_2(hfac)_4]\cdot 2MeOH$ (**1**), $[Cu_3Tb_2(H_3L)_2(OAc)_2(hfac)_4]\cdot 2EtOH$ (**2**) and $[Cu_3Tb_2(H_3L)_2(OAc)_2(hfac)_4]\cdot 2iso\text{-}C_3H_7OH$ (**3**), respectively; while $[Cu_3Tb_2(H_3L)_2(OAc)_2(hfac)_4]\cdot 2H_2O$ (**4**) was quantitatively transformed from complex **1** by taking place of methanol molecules with water molecules. In order to yield $[Cu_3Tb_2(H_3L)_2(OAc)_2(hfac)_4]$ SMMs with larger ROH lattice solvent molecules, other ROH solvents such as isobutyl alcohol, n-butyl alcohol and isoamyl alcohol were also used instead of methanol for **1**, but no any crystalline products could be obtained. Furthermore, the $[Cu_3Dy_2(H_3L)_2(OAc)_2(hfac)_4]$ SMM system was also explored, but only the crystal structure of $[Cu_3Dy_2(H_3L)_2(OAc)_2(hfac)_4]\cdot 2MeOH$ (**5**) was successfully solved, the crystal structure of $[Cu_3Dy_2(H_3L)_2(OAc)_2(hfac)_4]$ SMMs with other lattice solvent molecules (H_2O, ethanol and isopropyl alcohol) could not be obtained due to the severe twinning phenomenon.

Structural description. All $[Cu_3Tb_2(H_3L)_2(OAc)_2(hfac)_4]\cdot 2ROH$ SMMs have the main structure $[Cu_3Tb_2(H_3L)_2(OAc)_2(hfac)_4]$ (Fig. 2). Therefore, the structure of $[Cu_3Tb_2(H_3L)_2(OAc)_2(hfac)_4]\cdot 2MeOH$ (**1**) is chose to be described in detail. In the main structure $[Cu_3Tb_2(H_3L)_2(OAc)_2(hfac)_4]$, a $\{Cu_3(H_3L)_2\}$ linear unit is formed through bridging two terminal $\{Cu(H_3L)\}^-$ fragments using a central Cu^{2+} ion, then two Tb^{3+} ions link to this $\{Cu_3(H_3L)_2\}$ linear unit in the opposite direction, in which each Tb^{3+} ion connects with the central Cu^{2+} ion and one external Cu^{2+} ion through sharing one μ_3-O atom and one μ-O atom from one H_3L^{3-} ligand, and one μ_3-O atom from the other H_3L^{3-} ligand (Fig. 2a), similar to those in $\{Ln_2Cu_3(H_3L)_2X_n\}$[35]. The eight-coordinate sphere of each Tb^{3+} ion is finally completed by two $hfac^-$ anions and one OAc^- anion. Shape software[37] was adopted to calculate the Tb(III) coordination polyhedron, giving a triangular dodecahedron as the most likely configuration for complex **1**, and the deviation value from the ideal D_{2d} symmetry is 1.015 (Table S1, SI). It is worth noting that the Tb(III) coordination polyhedron can also be viewed as a biaugmented trigonal prism, but with the deviation value of 1.756 from the ideal D_{2d} symmetry. Moreover, the calculation result for the Tb(III) coordination polyhedra of complexes **2**–**4** using Shape software[37] are listed in Tables S2–S4 (SI), respectively.

The external Cu atom, in a distorted square-pyramidal configuration, is coordinated with two N atoms and two μ-O atoms from one H_3L^{3-} ligand, forming the base of the pyramid; whereas the third μ-O atom from the same H_3L^{3-} ligand occupying the apical site. The central Cu^{2+} ion is coordinated by two μ_3-O atoms and four μ-O atoms from two H_3L^{3-} ligands, generating a distorted octahedral geometry, in which two μ-O atoms bridging the central Cu atom and the external Cu atom are in the Jahn-Teller axis' direction, with the long Cu-O bond distance of 2.665 Å for complex **1**.

There are hydrogen bonds between the methanol O atom and the carboxylate O atom with the $O_{methanol}\cdots O_{carboxylate}$ distance of 2.803 Å and between the methanol O atom and the N atom from the H_3L^{3-} ligand with the $O_{methanol}\cdots N$ distance of 2.937 Å for complex **1**. Similar hydrogen bonds were observed between the ethanol O

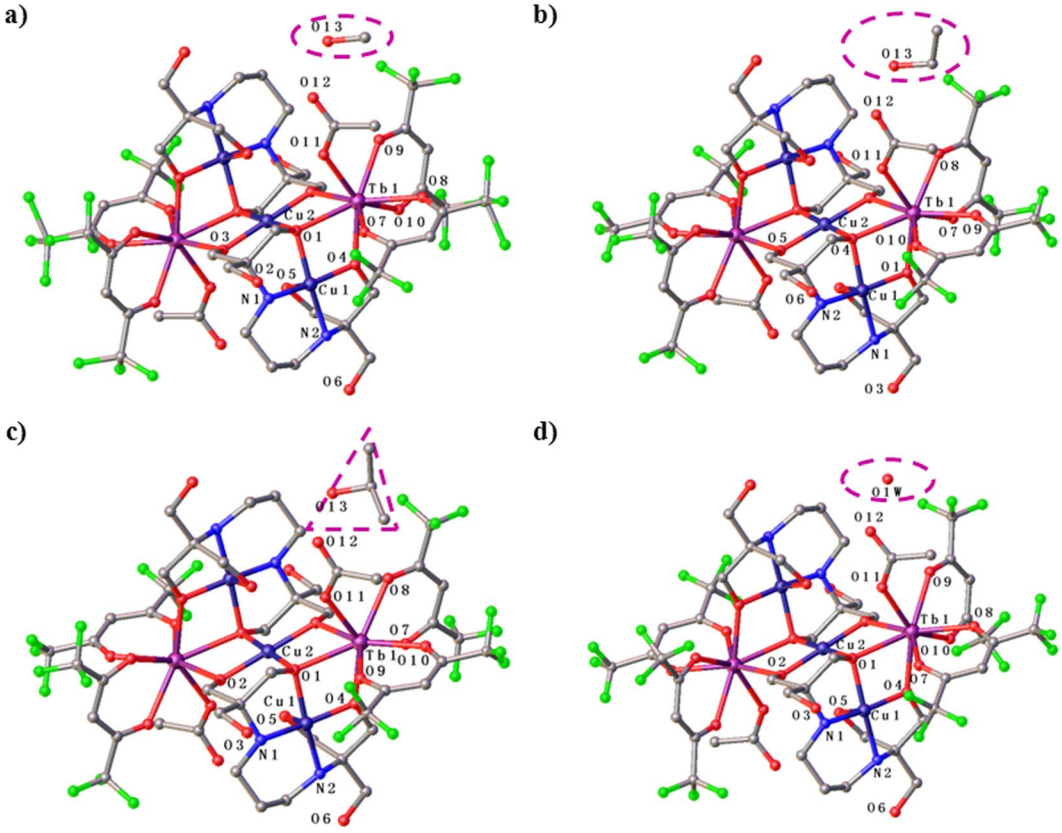

Figure 2. Crystal structures of **1** (**a**), **2** (**b**), **3** (**c**) and **4** (**d**). All lattice solvent molecules are highlighted, and all H atoms are omitted for clarity.

atom and the carboxylate O atom with the $O_{ethanol}\cdots O_{carboxylate}$ distance of 2.788 Å and between the ethanol O atom and the N atom from the H_3L^{3-} ligand with the $O_{ethanol}\cdots N$ distance of 2.941 Å for **2**; between the isopropyl alcohol O atom and the carboxylate O atom with the $O_{isopropyl\ alcohol}\cdots O_{carboxylate}$ distance of 2.817 Å and between the isopropyl alcohol O atom and the N atom from the H_3L^{3-} ligand with the $O_{isopropyl\ alcohol}\cdots N$ distance of 2.922 Å for **3**; and between the water O atom and the carboxylate O atom with the $O_{water}\cdots O_{carboxylate}$ distance of 2.866 Å and between the water O atom and the N atom from the H_3L^{3-} ligand with the $O_{water}\cdots N$ distance of 2.944 Å for **4**. These weak intermolecular interactions play important roles in not only stabilization of crystal structures but also adjustment of magnetic properties for complexes **1**–**4**.

Complex **5** has the same structure as **1**, but Dy instead of Tb is used (Fig. S1, SI). The Dy-O bond distance (average 2.357 Å) in **5** is slightly smaller than the Tb-O bond length (average 2.368 Å) in **1** owing to the lanthanide contraction effect. The Dy(III) coordination polyhedron can also be described as a triangular dodecahedron with the deviation value of 0.975 from the ideal D_{2d} symmetry (Table S5, SI). This value is a little smaller than that of **1** (1.015), indicating that the Dy(III) coordination polyhedron in **5** is closer to a triangular dodecahedron than the Tb(III) coordination polyhedron in **1**. The deviation value from the ideal D_{2d} symmetry for a biaugmented trigonal prism is 1.735 for **5**, also a little smaller than that of **1** (1.756). Similar to **1**, there are also hydrogen bonds between the methanol O atom and the carboxylate O atom with the $O_{methanol}\cdots O_{carboxylate}$ distance of 2.796 Å and between the methanol O atom and the N atom from the H_3L^{3-} ligand with the $O_{methanol}\cdots N$ distance of 2.937 Å for complex **5**.

Magnetic properties. The direct current (dc) variable-temperature magnetic susceptibility of complexes **1**–**4** was measured at 1000 Oe applied field (Fig. 3). The room temperature χT values of the complexes **1** (24.91 cm^3 K mol^{-1}), **2** (24.85 cm^3 K mol^{-1}), **3** (24.84 cm^3 K mol^{-1}) and **4** (24.90 cm^3 K mol^{-1}) are slightly larger than the theoretical value of 24.77 cm^3 K mol^{-1} for three noninteracting Cu^{2+} ions ($g = 2.0$) and two uncoupled Tb^{3+} ions ($^7F_6$, $J = 6$, $L = 3$, $S = 3$, $g = 3/2$). As shown in Fig. 3, upon cooling, the χT product almost keeps a constant value or just slightly lowers; however, below about 50 K, a rapid rise appears until reaches the maximum values of 53.92 cm^3 K mol^{-1} at 6.0 K for **1**, 45.14 cm^3 K mol^{-1} at 4.0 K for **2** and 49.80 cm^3 K mol^{-1} at 4.0 K for **3**; the χT values then decline to 49.34 cm^3 K mol^{-1} at 2.0 K for **1**, 43.48 cm^3 K mol^{-1} at 2.0 K for **2** and 47.48 cm^3 K mol^{-1} at 2.0 K for **3**. Exceptionally, complex **4** does not reach the maximum value until 2.0 K (44.60 cm^3 K mol^{-1}). These magnetic behaviours are very similar to those of $\{Tb_2Cu_3(H_3L)_2X_n\}$ ($X = OAc^-$ and NO_3^-)[35], suggesting that all four complexes are also ferromagnetic. The small difference in dc magnetic susceptibilities of **1**–**4** means that there is a solvatomagnetic effect in this $[Cu_3Tb_2(H_3L)_2(OAc)_2(hfac)_4]$ SMM system.

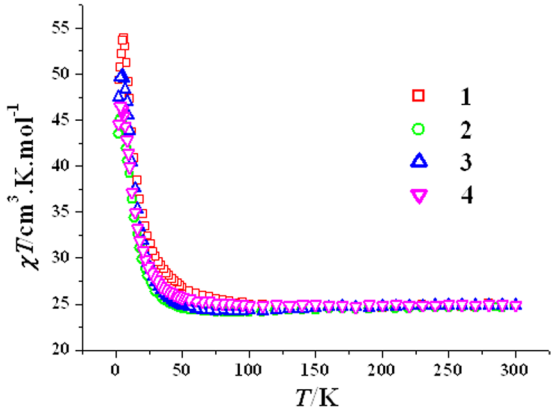

Figure 3. Plot of χT vs T for **1–4**.

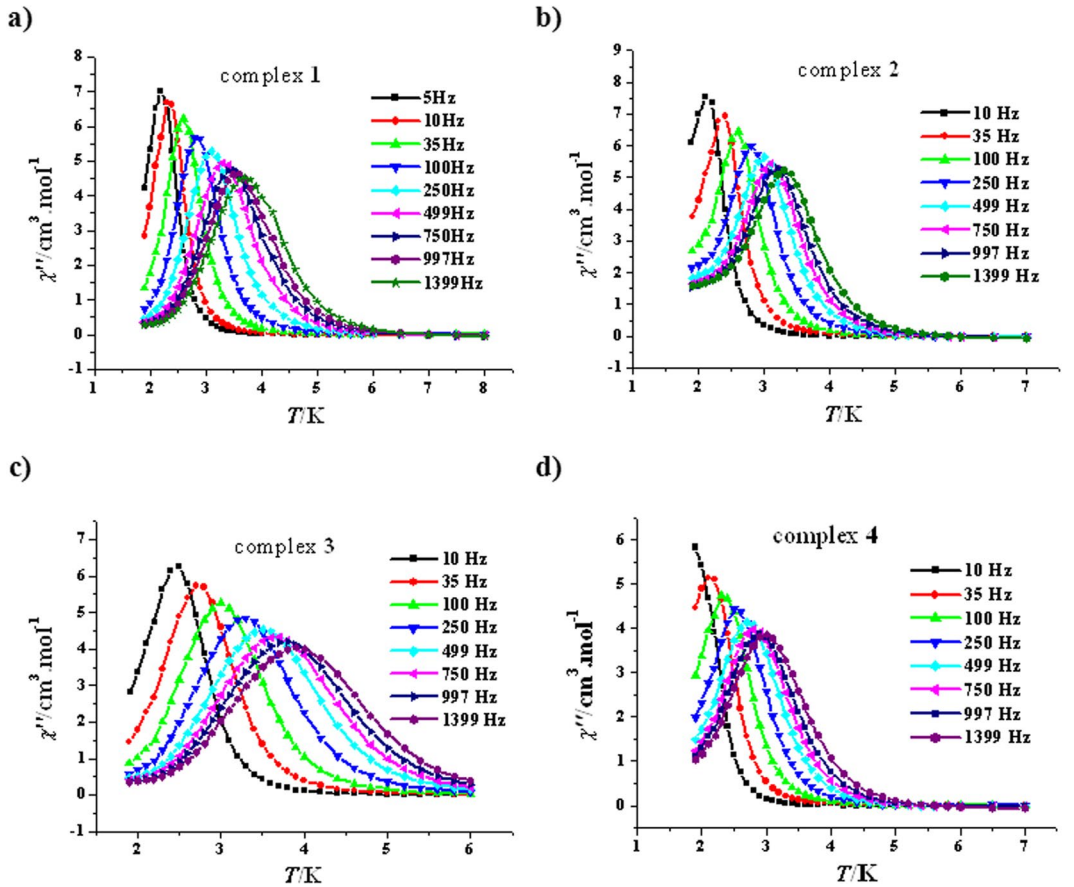

Figure 4. Plots of χ'' vs T for **1** (**a**), **2** (**b**), **3** (**c**) and **4** (**d**) ($H_{dc} = 0$ Oe, $H_{ac} = 2.5$ Oe).

The solvatomagnetic effect could also be detected by alternating current (ac) magnetic susceptibility investigations. Both the in-phase (χ', Fig. S2, SI) and the out-of-phase (χ'', Fig. 4) of variable-temperature ac magnetic susceptibility for **1–4** are frequency-dependent in zero dc field, indicating slow magnetic relaxation typical for SMMs. Such thermally induced relaxation was fitted with the Arrhenius law, $\tau = \tau_0 \exp(U_{eff}/kT)$, extracting U_{eff}/k values of 30.0(0.4) K for **1**, 32.4(0.2) K for **2**, 33.1(0.7) K for **3** and 25.7(0.2) K for **4** as well as τ_0 values of $3.7(0.2) \times 10^{-8}$ s for **1**, $6.2(0.1) \times 10^{-9}$ s for **2**, $2.6(0.3) \times 10^{-8}$ s for **3** and $2.3(0.1) \times 10^{-8}$ s for **4** (Fig. 5a). All four τ_0 values are within the normal range for SMMs/SIMs (10^{-5}–10^{-11} s)[13]. A comparison of the effective barrier value for complexes **1–4** with the R group of the ROH lattice solvent molecules (R = H, **4**; R = CH_3, **1**; R = C_2H_5, **2** and R = C_3H_7, **3**) reveals an important magneto-structural correlation for this $[Cu_3Tb_2(H_3L)_2(OAc)_2(hfac)_4]$ SMM system: The larger the R group in ROH, the higher the energy barrier of the $[Cu_3Tb_2(H_3L)_2(OAc)_2(hfac)_4]$·2ROH SMM (Fig. 5b). It is noteworthy that either the U_{eff}/k value of **2** or the U_{eff}/k value of **3** is one of the largest values so far for the Cu-Tb heterometallic SMMs in zero dc field, just smaller than

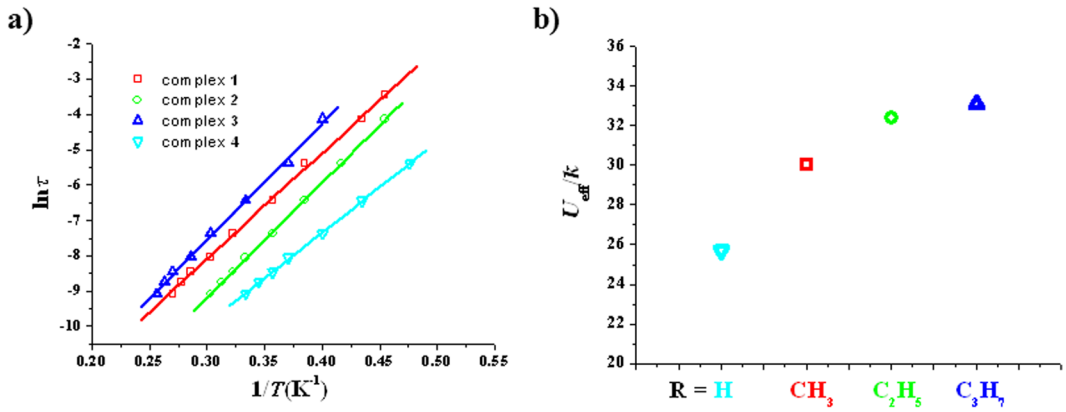

Figure 5. Plot of ln(τ) vs 1/T for **1–4** (**a**), the solid lines represent the best fitting with the Arrhénius law; magneto-structural correlation between U_{eff}/k values and the R groups of ROH solvent molecules (**b**).

complex	ROH solvent molecule	the deviation value of biaugmented trigonal prism for the Tb^{3+} ion	the shortest $Cu_{central}\cdots Cu_{central}$ separation	U_{eff}/k (K)	τ_0 (s)
4	R = H	1.735	10.042	25.7	2.3×10^{-8}
1	R = CH_3	1.756	10.086	30.0	3.7×10^{-8}
2	R = C_2H_5	1.584	10.244	32.4	6.2×10^{-9}
3	R = C_3H_7	1.496	10.309	33.1	2.6×10^{-8}

Table 1. Magneto-structural correlation of U_{eff}/k values with two structural parameters.

that of $(NMe_4)_2[Tb_2Cu_3(H_3L)_2(NO_3)_7(CH_3OH)_2](NO_3)$ (36 K)[35]; the U_{eff}/k value of **1** is also remarkable, which is comparable with that of $[Cu_2(valpn)_2Tb_2(N_3)_6]\cdot 2CH_3OH$ [H_2valpn = 1,3-propanediylbis(2-iminomethylene -6-methoxyphenol)] (30.1 K, $H_{dc} = 0$ Oe)[38]. In many cases[39–44], a dc field is necessary for 3d-4f heterometallic complexes to display magnetic relaxation because of the obvious quantum-tunnelling effects.

Simplified theoretical investigations by Murrie group suggested that the magnetic bistability in the $[Cu_3Tb_2(H_3L)_2X_n]$ system is not because of single-ion behaviours, and both the Cu···Cu and Cu···Tb ferromagnetic interactions maybe quench the tunnel splitting, which are similar to acting as an internal applied field, inducing to zero-field SMM behaviours[35]. Nevertheless, the difference of the Tb^{3+} coordination configurations has influence on the SMM characteristics[35]. Owing to great difficulty for theoretical calculation and comparison of the Cu···Cu and Cu···Tb ferromagnetic couplings[35], we tried to make a magneto-structural correlation for complexes **1–4** using the deviation value from the ideal D_{2d} symmetry of the biaugmented trigonal prism for the Tb^{3+} ion and the intermolecular distance as two main structural parameters. As shown in Table 1, the coordination configuration of the Tb^{3+} ions is closer to the biaugmented trigonal prism from **1** to **3**, the corresponding energy barrier value becomes larger from **1** to **3**, indicating the biaugmented trigonal prism configuration in the $[Cu_3Tb_2(H_3L)_2(OAc)_2(hfac)_4]$ SMM system is the dominant configuration; but **4** is a bit unusual, its deviation value (1.735) is comparable with that of **1** (1.756), which suggests that other structural factors such as intermolecular distances need to be considered; as shown in Table 1, the longer the intermolecular distance (defined by the shortest $Cu_{central}\cdots Cu_{central}$ separation), the higher the energy barrier; which is in line with the magneto-structural correlation using the R group itself, because larger ROH lattice solvent molecules may enhance intermolecular distances correspondingly.

The SMM properties of **1–4** were also evaluated by the parameter $\Phi = (\Delta T_f/T_f)/\Delta(\log f)$[45], where f represents the frequency and T_f the peak temperature of χ'' curve; the Φ values of **1, 2, 3** and **4** are 0.18, 0.17, 0.17 and 0.21, respectively, which support the superparamagnet behaviour of these SMMs ($\Phi > 0.1$), but exclude any spin glass properties ($\Phi \approx 0.01$)[45]. Further determinations of ac magnetic susceptibility revealed that the variable-frequency χ'' signals of **1–4** are evidently temperature-dependent (Fig. 6), confirming slow magnetic relaxation of SMMs. The χ'' vs χ' plots show classical half-circular curves for all four complexes, indicating a single magnetic relaxation process (Fig. S3, SI). These Cole-Cole plots could be fitted with a generalized Debye model[46,47]. The α values are smaller than 0.07 for **2–4**, suggesting a single relaxation mechanism; while the α values for **1** are from 0.10 to 0.22, indicating a relatively narrow distribution of the relaxation time. In addition, no any hysteresis was observed in the M vs H plot at 1.9 K for **1–4** (Fig. S4, SI).

The χT value at room temperature for complex **5** is 29.44 cm^3 K mol^{-1} (Fig. 7a), which is in good agreement with the expected value of 29.47 cm^3 K mol^{-1} for three uncoupled Cu^{2+} ions ($g = 2.0$) and two isolated Dy^{3+} ions ($^6H_{15/2}$, $J = 15/2$, $S = 5/2$, $L = 5$, $g = 4/3$). When temperature is decreased, the χT product decreases very slowly until 110 K (29.20 cm^3 K mol^{-1}), then increases very gently until about 50 K. Below this temperature, the χT value rises rapidly, reaching the maximum of 63.92 cm^3 K mol^{-1} at 5 K and then dropping down to 62.38 cm^3 K mol^{-1} at 2 K, these magnetic behaviors are similar to those for **1** and $(NMe_4)_2\{Dy_2Cu_3(NO_3)_7(CH_3OH)_2\}(NO_3)$[35], and the ferromagnetic coupling obviously exists between the Cu^{2+} ion and the Dy^{3+} ion as well as among the Cu^{2+} ions, similar to that observed in $[Gd_2Cu_3(H_3L)_2(CH_3COO)_6]\cdot THF\cdot 3H_2O$ by Murrie group[35].

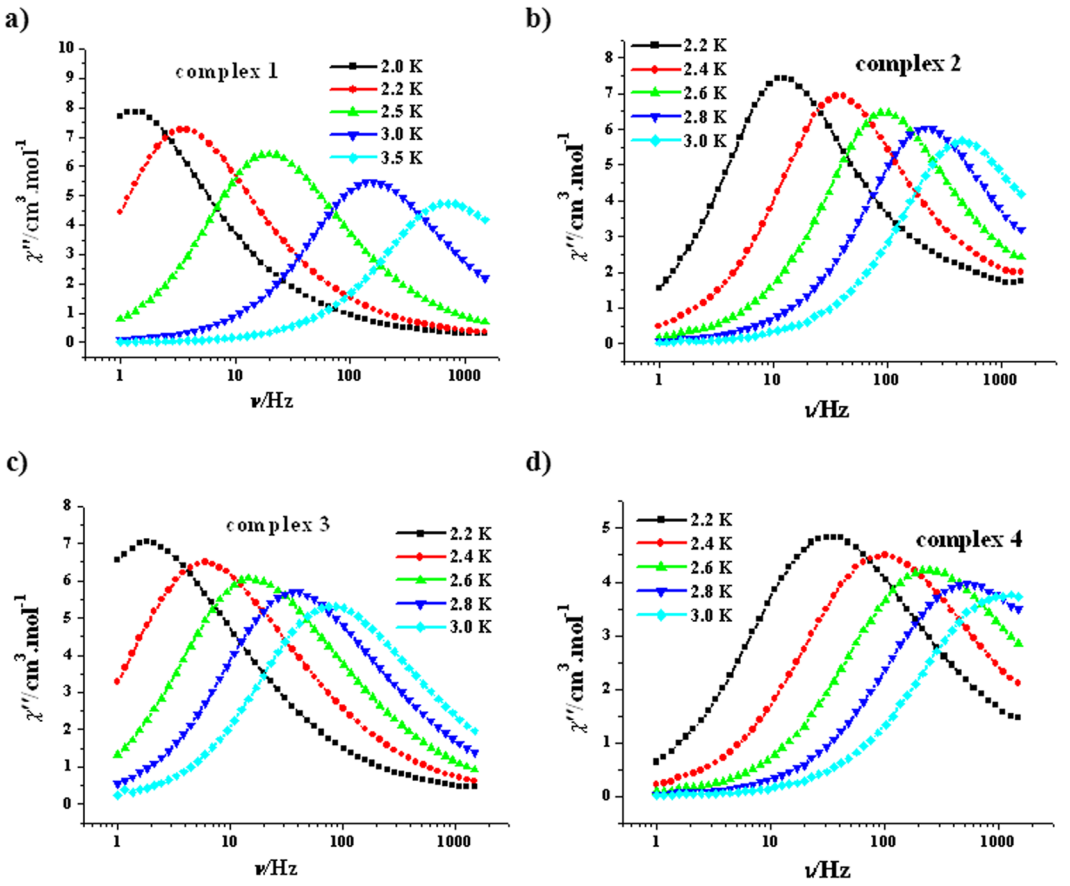

Figure 6. Plots of χ'' vs ν for **1** (**a**), **2** (**b**), **3** (**c**) and **4** (**d**) ($H_{dc} = 0$ Oe, $H_{ac} = 2.5$ Oe).

The magnetization dynamics of compound **5** are similar to those of complexes **1**–**4**. Under zero dc field, the appearance of frequency-dependent χ' (Fig. S5, SI) and χ'' signals (Fig. 7b) indicates SMM behaviors of **5**. The SMM parameters extracted from the Arrhenius law for **5** are $U_{eff}/k = 30.0(0.2)$ K and $\tau_0 = 9.7(0.1) \times 10^{-9}$ s (Fig. 7c). The energy barrier value of **5** is comparable with that of **1**, but obviously larger than that of $(NMe_4)_2\{Dy_2Cu_3(H_3L)_2(NO_3)_7(CH_3OH)_2\](NO_3)$ [23.9(0.1) K], whose χ'' signals even do not appear peaks in zero dc field[35]. Notably, this U_{eff}/k value is the third high value for the Cu-Dy heterometallic SMMs, after 47 K of $[\{Dy(hfac)_3\}_2\{Cu(dpk)_2\}]$ (dpk^- = di-2-pyridyl ketoximate)[48] and 41.6 K of $[Cu_4Dy_4(vanox)_6(Hvanox)_2(NO_3)_4(\mu\text{-}HOMe)_2]\cdot 6MeOH$ (H_2vanox = 3-methoxy-2-hydroxybenzaldoxime)[49]. Furthermore, this U_{eff}/k value is remarkable larger than those of the Cu-Dy heterometallic SMMs with higher nucleus (<20 K)[50,51]. Additionally, the parameter Φ value of 0.16 for **5** supports the SMM nature too.

The variable-frequency ac magnetic susceptibility study of **5** revealed that the χ'' signals of **5** are temperature-dependent (Fig. 7d), confirming the SMM behavior of **5**. The Cole-Cole plots were fitted to a generalized Debye model (Fig. S6, SI)[46,47], giving the α values of 0.01–0.08 for **5**, suggesting the magnetic relaxation happens *via* a single relaxation process. Additionally, the *M* vs *H* plot of **5** shows no any hysteresis at 1.9 K (Fig. S7, SI).

Conclusions

In summary, a mixed OAc^-/$hfac^-$ co-ligands' synthesis strategy was adopted to prepare 3d-4f heterometallic SMMs based on the 1,3-Bis[tris(hydroxymethyl)methylamino]propane ligand (H_6L). The ROH lattice solvent molecules (R = H, CH_3, C_2H_5 and C_3H_7) in the $[Cu_3Tb_2(H_3L)_2(OAc)_2(hfac)_4]$ SMM system have great influences on the energy barrier; the larger the R group, the higher the energy barrier. We predict that the larger ROH molecule may enlarge the intermolecular distance and can help to change the coordination configuration of the Ln(III) ions through the hydrogen bonding interaction between the ROH lattice solvent molecule and the $[Cu_3Tb_2(H_3L)_2(OAc)_2(hfac)_4]$ main-structural molecule. Our work demonstrates that solvatomagnetic effects can be used to continuously fine-tune energy barriers in SMMs. The discovery is bound to have significances in enhancing and turning energy barriers of molecular nanomagnets *via* chemical methods such as using lattice-solvent effects.

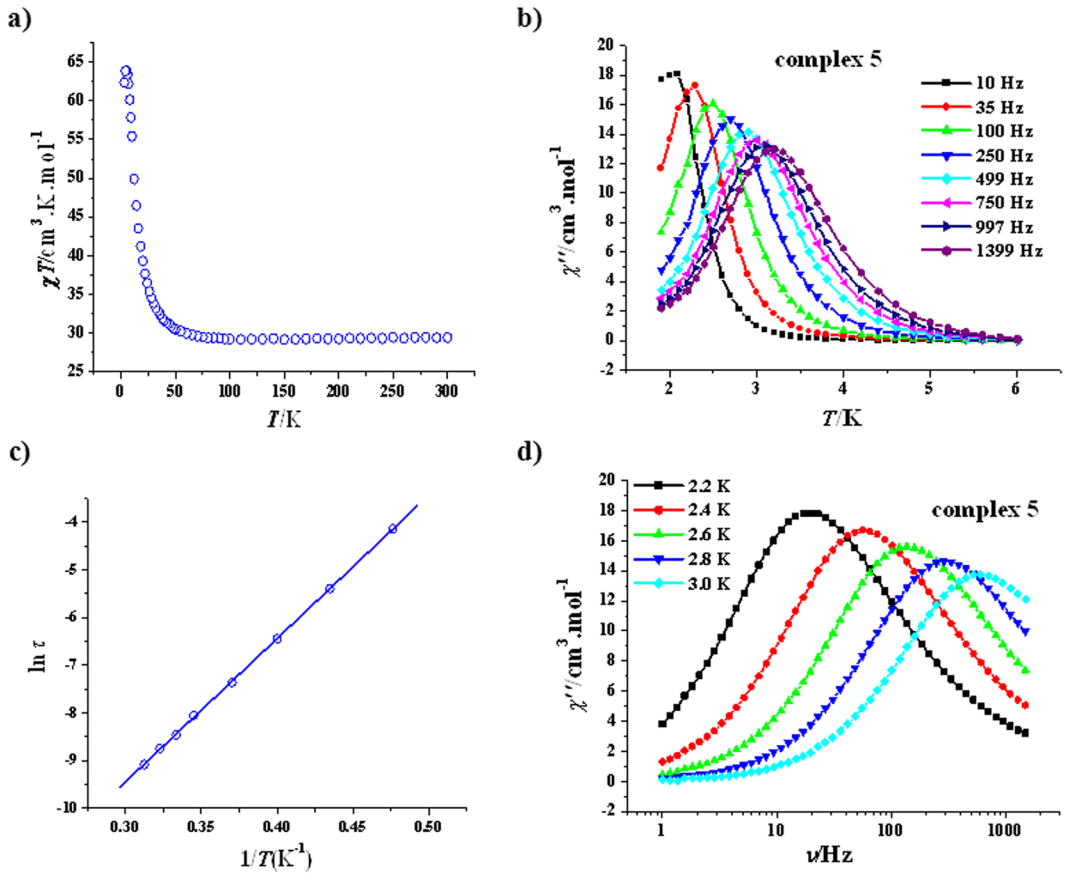

Figure 7. Plot of χT vs T of **5** (**a**); plot of χ'' vs T for **5** (**b**) ($H_{dc} = 0$ Oe, $H_{ac} = 2.5$ Oe); plot of $\ln(\tau)$ vs $1/T$ for **5** (**c**), the solid line represents the best fitting with the Arrhénius law; plot of χ'' vs ν for **5** (**d**) ($H_{dc} = 0$ Oe, $H_{ac} = 2.5$ Oe).

Methods

Physical measurements. The elemental analyses were measured on a Vario ELIII elemental analyser. The magnetic susceptibility measurements were carried out on a Quantum Design MPMS-XL5 SQUID magnetometer, and diamagnetic corrections were calculated from Pascal's constants of all components.

Synthesis of $[Cu_3Tb_2(H_3L)_2(OAc)_2(hfac)_4]\cdot 2MeOH$ (1). To a mixture of H_6L (0.25 mmol) and $Cu(ClO_4)_2\cdot 6H_2O$ (0.375 mmol) in 20 mL of MeOH, was added $Tb(OAc)(hfac)_2(H_2O)_2$ (0.15 mmol), a blue solution was formed after being stirred for 10 min; Et_3N (0.75 mmol) was then added dropwise, the resultant solution was stirred for 3 h at room temperature and turned violet. Violet plate-like X-ray quality crystals were obtained through slow evaporation of the filtrate at room temperature over 1 week. Yield (25%). Anal. Calcd (%) for $C_{48}H_{64}Cu_3F_{24}N_4O_{26}Tb_2$ (**1**) C 27.75; H 3.11; N 2.70. Found: C 27.80; H 3.14; N 2.67.

Synthesis of $[Cu_3Tb_2(H_3L)_2(OAc)_2(hfac)_4]\cdot 2EtOH$ (2). The same synthetic procedure for complex **1** was followed, but using ethanol instead of methanol. Violet plate-like X-ray quality crystals were obtained through slow evaporation of the filtrate at room temperature over 10 days. Yield (27%). Anal. Calcd (%) for $C_{50}H_{68}Cu_3F_{24}N_4O_{26}Tb_2$ (**2**): C 28.52; H 3.26; N 2.66. Found: C 28.55; H 3.29; N 2.63.

Synthesis of $[Cu_3Tb_2(H_3L)_2(OAc)_2(hfac)_4]\cdot 2iso\text{-}C_3H_7OH$ (3). The same synthetic procedure for complex **1** was followed, but using isopropyl alcohol instead of methanol. Violet plate-like X-ray quality crystals were obtained through slow evaporation of the filtrate at room temperature over 15 days. Yield (22%). Anal. Calcd (%) for $C_{52}H_{72}Cu_3F_{24}N_4O_{26}Tb_2$ (**3**): C 29.27; H 3.40; N 2.63. Found: C 29.23; H 3.43; N 2.60.

Synthesis of $[Cu_3Tb_2(H_3L)_2(OAc)_2(hfac)_4]\cdot 2H_2O$ (4). Complex **1** was kept at 60 °C for 6 h, and then exposed on air for 24 h. Violet plate-like X-ray quality crystals of **4** were obtained quantitatively. Anal. Calcd (%) for $C_{46}H_{60}Cu_3F_{24}N_4O_{26}Tb_2$ (**4**): C 26.96; H 2.95; N 2.73. Found: C 27.02; H 2.99; N 2.69.

Synthesis of $[Cu_3Dy_2(H_3L)_2(OAc)_2(hfac)_4]\cdot 2MeOH$ (5). The same synthetic procedure for complex **1** was followed, but using $Dy(OAc)(hfac)_2(H_2O)_2$ instead of $Tb(OAc)(hfac)_2(H_2O)_2$. Violet plate-like X-ray quality crystals were obtained through slow evaporation of the filtrate at room temperature over 1 week. Yield (28%). Anal. Calcd (%) for $C_{48}H_{64}Cu_3Dy_2F_{24}N_4O_{26}$ (**5**): C 27.66; H 3.09; N 2.69. Found: C 27.69; H 3.11; N 2.67.

X-ray crystallography. A single crystal with dimensions $0.261 \times 0.093 \times 0.025\,mm^3$ of **1**, $0.178 \times 0.063 \times 0.024\,mm^3$ of **2**, $0.183 \times 0.125 \times 0.031\,mm^3$ of **3**, $0.108 \times 0.067 \times 0.025\,mm^3$ of **4**, and $0.134 \times 0.125 \times 0.027\,mm^3$ of **5** was picked out to mount on a Bruker SMART APEX-CCD diffractometer with Mo-K_α radiation ($\lambda = 0.71073$ Å) for data collection at 173(2) K. Empirical absorption corrections from φ and ω scan were applied. Cell parameters were calculated by the global refinement of the positions of all collected reflections for five complexes. The structures were solved by direct methods and refined by a full matrix least-squares technique based on F^2 using with the SHELX-2014 program package. All hydrogen atoms were set in calculated positions and refined as riding atoms, and all non-hydrogen atoms were refined anisotropically. CCDC 1574978–1574982 contain the supplementary crystallographic data, which can be obtained free of charge from the Cambridge Crystallographic Data Centre via www.ccdc.cam.ac.uk/data_request/cif.

Crystal data for **1**: $P-1$, $a = 10.086(2)$ Å, $b = 12.463(3)$ Å, $c = 15.594(3)$ Å, $\alpha = 104.67(3)°$, $\beta = 94.07(3)°$, $\gamma = 108.97(3)°$, $V = 1767.9(7)$ Å^3, $M_r = 2077.49$, $D_c = 1.951\,g\,cm^{-3}$, $Z = 1$, $R_1 = 0.0366$ ($I > 2\sigma(I)$), $wR_2 = 0.0878$ ($I > 2\sigma(I)$), $S = 1.080$.

Crystal data for **2**: $P-1$, $a = 10.243(2)$ Å, $b = 12.469(3)$ Å, $c = 15.602(3)$ Å, $\alpha = 101.71(3)°$, $\beta = 96.50(3)°$, $\gamma = 110.00(3)°$, $V = 1797.2(6)$ Å^3, $M_r = 2105.54$, $D_c = 1.945\,g\,cm^{-3}$, $Z = 1$, $R_1 = 0.0498$ ($I > 2\sigma(I)$), $wR_2 = 0.1085$ ($I > 2\sigma(I)$), $S = 1.122$.

Crystal data for **3**: $P-1$, $a = 10.309(2)$ Å, $b = 12.473(3)$ Å, $c = 15.677(3)$ Å, $\alpha = 101.80(3)°$, $\beta = 96.96(3)°$, $\gamma = 110.19(3)°$, $V = 1811.4(7)$ Å^3, $M_r = 2133.58$, $D_c = 1.956\,g\,cm^{-3}$, $Z = 1$, $R_1 = 0.0345$ ($I > 2\sigma(I)$), $wR_2 = 0.0797$ ($I > 2\sigma(I)$), $S = 1.084$.

Crystal data for **4**: $P-1$, $a = 10.042(2)$ Å, $b = 12.480(3)$ Å, $c = 15.819(3)$ Å, $\alpha = 107.08(3)°$, $\beta = 99.23(3)°$, $\gamma = 109.83(3)°$, $V = 1706.2(7)$ Å^3, $M_r = 2049.44$, $D_c = 1.995\,g\,cm^{-3}$, $Z = 1$, $R_1 = 0.0488$ ($I > 2\sigma(I)$), $wR_2 = 0.0945$ ($I > 2\sigma(I)$), $S = 1.153$.

Crystal data for **5**: $P-1$, $a = 10.085(2)$ Å, $b = 12.427(3)$ Å, $c = 15.581(3)$ Å, $\alpha = 104.59(3)°$, $\beta = 94.21(3)°$, $\gamma = 108.86(3)°$, $V = 1762.5(7)$ Å^3, $M_r = 2084.65$, $D_c = 1.964\,g\,cm^{-3}$, $Z = 1$, $R_1 = 0.0321$ ($I > 2\sigma(I)$), $wR_2 = 0.0762$ ($I > 2\sigma(I)$), $S = 1.074$.

References

1. Milios, C. J. *et al.* A Record Anisotropy Barrier for a Single-Molecule Magnet. *J. Am. Chem. Soc.* **129**, 2754–2755 (2007).
2. Xu, H.-B. *et al.* Stringing Oxo-Centered Trinuclear [Mn^{III}_3O] Units into Single-Chain Magnets with Formate or Azide Linkers. *Angew. Chem. Int. Ed. 2007* **46**, 7388–7392 (2007).
3. Bai, Y.-L. *et al.* Coexistence of Magnetization Relaxation and Dielectric Relaxation in a Single-Chain Magnet. *J. Am. Chem. Soc.* **128**, 16428–16429 (2006).
4. Liu, C.-M. *et al.* 1D Coordination Polymers Constructed from anti-anti Carboxylato-Bridged $Mn^{III}_3O(Brppz)_3$ Units: From Long-Range Magnetic Ordering to Single-Chain Magnet Behaviors. *Inorg. Chem.* **48**, 4980–4987 (2009).
5. Halder, G. J. *et al.* Guest-dependent spin crossover in a nanoporous molecular framework material. *Science* **298**, 1762–1765 (2002).
6. Maspoch, D. *et al.* A nanoporous molecular magnet with reversible solvent-induced mechanical and magnetic properties. *Nat. Mater.* **2**, 190–195 (2003).
7. Rujiwatra, A. *et al.* Layered Cobalt Hydroxysulfates with Both Rigid and Flexible Organic Pillars: Synthesis, Structure, Porosity, and Cooperative Magnetism. *J. Am. Chem. Soc.* **123**, 10584–10594 (2001).
8. Sato, Y. *et al.* Solvatomagnetism-Induced Faraday Effect in a Cobalt Hexacyanochromate-Based Magnet. *J. Am. Chem. Soc.* **125**, 14590–14595 (2003).
9. Zhang, X.-M. *et al.* Dehydration-Induced Conversion from a Single-Chain Magnet into a Metamagnet in a Homometallic Nanoporous Metal-Organic Framework. *Angew. Chem. Int. Ed.* **46**, 3456–3459 (2007).
10. Liu, C.-M. *et al.* Solvatomagnetic effect and spin-glass behavior in a 1D coordination polymer constructed from EE-azido bridged Mn^{III}_3O units. *Chem. Commun.* **44**, 368–370 (2008).
11. Liu, C.-M. *et al.* A Chinese Pane-Like 2D Metal-Organic Framework Showing Magnetic Relaxation and Luminescence Dual-Functions. *Sci. Rep.* **7**, 11156, https://doi.org/10.1038/s41598-017-11006-5 (2017).
12. Sessoli, R. *et al.* Magnetic bistability in a metal-ion cluster. *Nature* **365**, 141–143 (1993).
13. Woodruff, D. N., Winpenny, R. E. P. & Layfield, R. A. Lanthanide single-molecule magnets. *Chem. Rev.* **113**, 5110–5148 (2013).
14. Bogani, L. & Wernsdorfer, W. Molecular spintronics using single-molecule magnets. *Nat. Mater.* **7**, 179–186 (2008).
15. Komeda, T. *et al.* Observation and electric current control of a local spin in a single-molecule magnet. *Nat. Commun.* **2**, 217 (2011).
16. Fetoh, A. *et al.* Photo-activation of single molecule magnet behavior in a manganese based complex. *Sci. Rep.* **6**, 23785, https://doi.org/10.1038/srep23785 (2016).
17. Gao, F. *et al.* Tetrathiafulvalene-supported triple-decker phthalocyaninato dysprosium(III) complex: synthesis, properties and surface assembly. *Sci. Rep.* **4**, 5928, https://doi.org/10.1038/srep05928 (2014).
18. Liu, J. *et al.* A Stable Pentagonal Bipyramidal Dy(III) Single-Ion Magnet with a Record Magnetization Reversal Barrier over 1000 K. *J. Am. Chem. Soc.* **138**, 5441–5450 (2016).
19. Yao, X.-N. *et al.* Two-Coordinate Co(II) Imido Complexes as Outstanding Single Molecule Magnets. *J. Am. Chem. Soc.* **139**, 373–380 (2017).
20. Ding, Y.-S. *et al.* On Approaching the Limit of Molecular Magnetic Anisotropy: A Near-Perfect Pentagonal Bipyramidal Dysprosium(III) Single-Molecule Magnet. *Angew. Chem. Int. Ed.* **55**, 16071–16074 (2016).
21. Goodwin, C. A. P. *et al.* Molecular magnetic hysteresis at 60 kelvin in dysprosocenium. *Nature* **548**, 439–442 (2017).
22. Qian, K. *et al.* A Single-Molecule Magnet Based on Heptacyanomolybdate with the Highest Energy Barrier for a Cyanide Compound. *J. Am. Chem. Soc.* **135**, 13302–13305 (2013).
23. Langley, S. K. *et al.* Modulation of slow magnetic relaxation by tuning magnetic exchange in {Cr_2Dy_2} single molecule magnets. *Chem. Sci.* **5**, 3246–3256 (2014).
24. Li, X.-L. *et al.* Modulation of Homochiral Dy^{III} Complexes: Single-Molecule Magnets with Ferroelectric Properties. *Chem.-Eur. J.* **18**, 14632–14637 (2012).
25. Zhang, L. *et al.* Anions Influence the Relaxation Dynamics of Mono-μ^3-OH-Capped Triangular Dysprosium Aggregates. *Inorg. Chem.* **54**, 5571–5578 (2015).
26. Liu, C.-M. *et al.* Simultaneous assembly of mononuclear and dinuclear dysprosium(III) complexes behaving as single-molecule magnets in a one-pot hydrothermal synthesis. *Sci. China Chem.* **60**, 358–365 (2017).
27. Habib, F. *et al.* Significant Enhancement of Energy Barriers in Dinuclear Dysprosium Single-Molecule Magnets Through Electron-Withdrawing Effects. *J. Am. Chem. Soc.* **135**, 13242–13245 (2013).
28. Wang, Y.-L. *et al.* Anions Influence the Relaxation Dynamics of Mono-μ3-OH-Capped Triangular Dysprosium Aggregates. *Inorg. Chem.* **55**, 5571–5578 (2016).

29. Zhang, X. *et al*. Influence of Guest Exchange on the Magnetization Dynamics of Dilanthanide Single-Molecule-Magnet Nodes within a Metal-Organic Framework. *Angew. Chem. Int. Ed.* **54**, 9861–9865 (2015).
30. Vallejo, J. *et al*. Guest-dependent single-ion magnet behaviour in a cobalt(II) metal-organic framework. *Chem. Sci.* **7**, 2286–2293 (2016).
31. Ferguson, A. *et al*. Bis-Tris Propane as a New Polydentate Linker in the Synthesis of Iron(III) and Manganese(II/III) Complexes. *Inorg. Chem.* **47**, 9742–9744 (2008).
32. Milway, V. A. *et al*. Directed Synthesis of $\{Mn_{18}Cu_6\}$ Heterometallic Complexes. *Angew. Chem. Int. Ed.* **52**, 1949–1952 (2013).
33. Liu, C.-M. *et al*. A single-molecule magnet featuring a parallelogram $[Dy_4(OCH_2-)_4]$ core and two magnetic relaxation processes. *Dalton Trans.* **42**, 14813–14818 (2013).
34. Han, S.-D. *et al*. Synthesis and Magnetic Properties of a Series of Octanuclear $[Fe_6Ln_2]$ Nanoclusters. *Cryst. Growth Des.* **15**, 2253–2259 (2015).
35. Ojea, M. J. H. *et al*. Enhancement of Tb^{III}-Cu^{II} Single-Molecule Magnet Performance through Structural Modification. *Chem.-Eur. J.* **22**, 12839–12848 (2016).
36. Liu, C.-M. *et al*. Hexanuclear $[Ni_2Ln_4]$ clusters exhibiting enhanced magnetocaloric effect and slow magnetic relaxation. *RSC Adv.* **4**, 53870–53876 (2014).
37. Casanova, D. *et al*. The rich stereochemistry of eight-vertex polyhedra: a continuous shape measures study. *Chem.-Eur. J.* **11**, 1479–1494 (2005).
38. Huang, X.-C. *et al*. End-On Azido-Bridged 3d-4f Complexes Showing Single-Molecule Magnet Property. *Inorg. Chem.* **52**, 7314–7316 (2013).
39. Kajiwara, T. *et al*. Structural Design of Easy-Axis Magnetic Anisotropy and Determination of Anisotropic Parameters of Ln^{III}-Cu^{II} Single-Molecule Magnets. *Chem. Eur. J.* **17**, 196–205 (2011).
40. Wen, H.-R. *et al*. Temperature-controlled polymorphism of chiral Cu^{II}-Ln^{III} dinuclear complexes exhibiting slow magnetic relaxation. *Dalton Trans.* **44**, 11191–11201 (2015).
41. Costes, J.-P. *et al*. Heterodinuclear Cu-Tb Single-Molecule Magnet. *Inorg. Chem.* **45**, 5–7 (2006).
42. Zhu, Q. *et al*. A series of goblet-like heterometallic pentanuclear $[Ln^{III}Cu^{II}_4]$ clusters featuring ferromagnetic coupling and single-molecule magnet behavior. *Chem. Commun.* **48**, 10736–10738 (2012).
43. Ishida, T. *et al*. Exchange coupling in TbCu and DyCu single-molecule magnets and related lanthanide and vanadium analogs. *Dalton Trans.* **41**, 13609–13619 (2012).
44. Wen, H.-R. *et al*. A family of nickel-lanthanide heterometallic dinuclear complexes derived from a chiral Schiff-base ligand exhibiting single-molecule magnet behaviors. *Inorg. Chim. Acta* **435**, 274–282 (2015).
45. Mydosh, J. A. Spin Glasses, An Experimental Introduction; Taylor and Francis Ltd.: London, pp. 1–256 (1993).
46. Cole, K. S. & Cole, R. H. Dispersion and absorption in dielectrics I. Alternating current characteristics. *J. Chem. Phys.* **9**, 341–351 (1941).
47. Aubin, S. M. *et al*. Reduced anionic Mn_{12} molecules with half-integer ground states as single-molecule magnets. *Inorg. Chem.* **38**, 5329–5340 (1999).
48. Mori, F. *et al*. Oximate-bridged trinuclear Dy-Cu-Dy complex behaving as a single-molecule magnet and its mechanistic investigation. *J. Am. Chem. Soc.* **128**, 1440–1441 (2006).
49. Kuhne, I. A. *et al*. An octanuclear $\{Cu^{II}_4Dy^{III}_4\}$ coordination cluster showing single molecule magnet behaviour from field accessible states. *Chem. Commun.* **50**, 1882–1885 (2014).
50. Liu, J.-L. *et al*. Two 3d-4f nanomagnets formed *via* a two-step in *situ* reaction of picolinaldehyde. *Chem. Commun.* **49**, 6549–6551 (2013).
51. Xue, S. *et al*. Molecular Magnetic Investigation of a Family of Octanuclear $[Cu_6Ln_2]$ Nanoclusters. *Inorg. Chem.* **53**, 8165–8171 (2014).

Acknowledgements

This work was supported by the National Key Basic Re-search Program of China (2013CB933403), the National Natural Science Foundation of China (21471154 and 91022014), and the Strategic Priority Research Program of the Chinese Academy of Sciences (XDB12010103).

Author Contributions

C.-M. Liu designed the concept. C.-M. Liu wrote the paper. C.-M. Liu, D.-Q. Zhang and D.-B. Zhu carried out the experimental work, and analyzed the results and revised the paper.

Additional Information

Supplementary information accompanies this paper at https://doi.org/10.1038/s41598-017-15852-1.

Competing Interests: The authors declare that they have no competing interests.

Publisher's note: Springer Nature remains neutral with regard to jurisdictional claims in published maps and institutional affiliations.